Title

THE LIMITING-CURRENT TECHNIQUE AT A SECTIONED ELECTRODE FOR THE STUDY OF BUOYANCY-INDUCED CONVECTION

Authors

Whitney, G.M.
Tobias, C.W.

Publication Date

1986-08-01

Lawrence Berkeley Laboratory

UNIVERSITY OF CALIFORNIA

Materials & Molecular Research Division

To be presented at American Society of Mechanical Engineers, Winter Annual Meeting, Anaheim, CA, December, 1986; and to be published in the ASME Symposium Volume, "Significant Questions in Buoyancy-Affected Enclosure or Cavity Flows"

THE LIMITING-CURRENT TECHNIQUE AT A SECTIONED ELECTRODE FOR THE STUDY OF BUOYANCY-INDUCED CONVECTION

G.M. Whitney and C.W. Tobias

August 1986

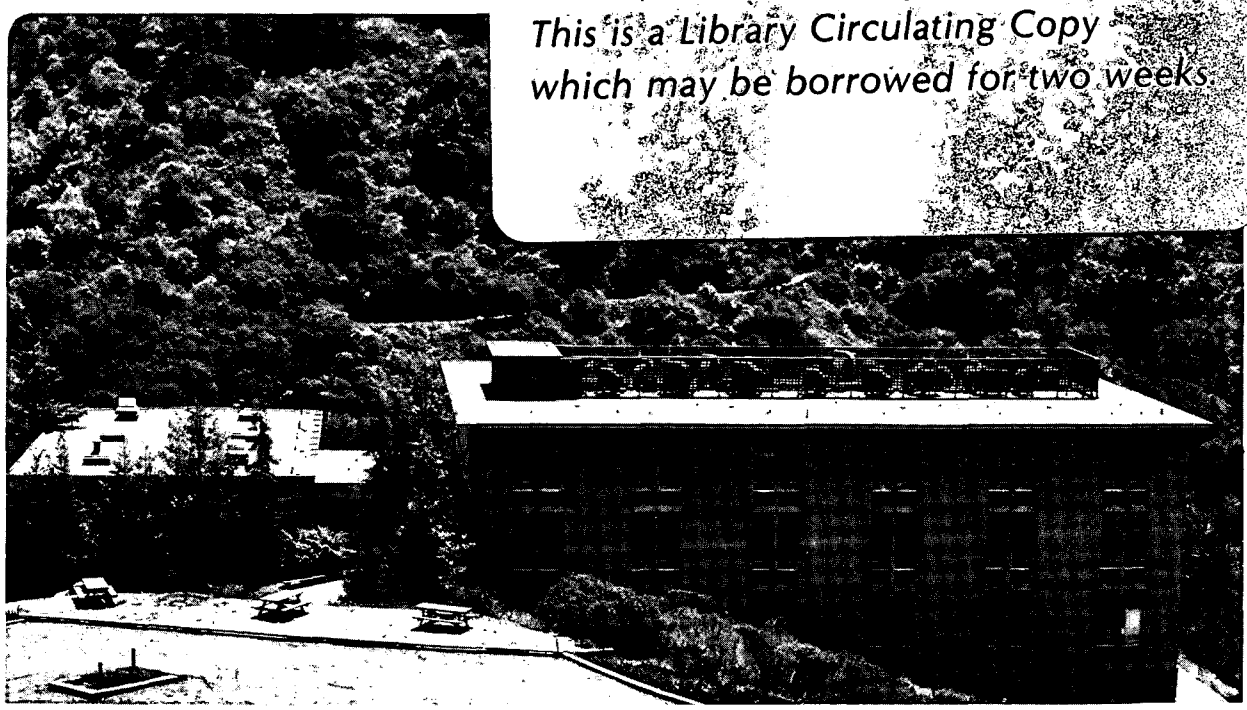

Prepared for the U.S. Department of Energy under Contract DE-AC03-76SF00098

DISCLAIMER

LBL-22036

The Limiting-Current Technique at a Sectioned Electrode for the Study of Buoyancy-Induced Convection

Gina M. Whitney

and

Charles W. Tobias

Department of Chemical Engineering,
University of California
and
Materials and Molecular Research Division,
Lawrence Berkeley Laboratory,
Berkeley, California 94720

August 1986

The Limiting-Current Technique at a Sectioned Electrode for the Study of Buoyancy-Induced Convection

Gina M. Whitney and Charles W. Tobias

Abstract

The onset of convective motion is investigated for a case in which the density profile is evolving in time in a semi-infinite fluid, due to a step change in surface concentration at a rigid, conducting boundary. The limiting current technique at a micro-mosaic electrode, which is composed of 100-μm, square elements, is used to effect the concentration change and to monitor the resulting mass transfer. The equations of transient mass transport by diffusion and migration and the equation of electroneutrality are solved numerically to determine the concentration and density profiles before the onset of convection. The critical Rayleigh number, based on the penetration depth of the concentration profile, was found to be approximately 1350 and to increase with increasing size and decreasing sensitivity of the sensing element.

Nomenclature

c_i	concentration of species i, mol /cm ^{3}
D_i	diffusivity of species i, cm ^{2}/sec
F	Faraday's constant, 96,487 C/equiv
h	total liquid depth, cm
i	current density, A/cm ^{2}
l	linear-segment penetration depth, defined in Eq. (1), cm
l_c	linear-segment penetration depth, based on concentration, cm
l_m	linear-segment penetration depth, based on density profile, cm
n	number of electrons participating in the electrode reaction
Nu	Nusselt number, dimensionless thermal energy flux
Pr	Prandtl number, ν/α
R	universal gas constant, 8.3143 J/mol-K
Ra	Rayleigh number
s_i	stoichiometric coefficient of species i in the electrode reaction
Sc	Schmidt number, ν/D_R
Sh	Sherwood number, dimensionless mass flux
t	time, sec
T	temperature, K
u_i	mobility of species i, cm ^{2}-mol/J-sec
y	vertical distance from electrode surface, cm
z_i	charge number of species i
α	thermal diffusivity, cm ^{2}/sec
α_i	densification coefficient of species i, (mol / cm ^{3})$^{-1}$
δ	nominal penetration depth $= \sqrt{\alpha t}$, cm
η	similarity variable for semi-infinite diffusion
ϕ	potential, volt
ν	kinematic viscosity, cm ^{2}/sec
ρ	density, g/cm ^{3}

Subscripts and superscripts

c	referring to time of convection onset
l	Ra based on linear-segment penetration depth
m	y at the density maximum Ra based on equivalent buoyant force to y_m
R	limiting reactant
t	Ra based on nominal penetration depth δ
0	at the electrode surface
∞	in the bulk solution

Introduction

An adverse density gradient in a horizontal fluid may induce convection if it is of sufficient magnitude and extends over a sufficient distance. The criterion for the onset of convection in such a fluid confined between two rigid boundaries with a linear density profile has become known as the Bénard-Rayleigh stability problem. Bénard-Rayleigh instability can result from temperature or concentration gradients. We consider here a variation of the Bénard-Rayleigh problem in which the density profile is nonlinear, time-dependent, and does not extend far enough into the fluid to be affected by the presence of the second boundary. This type of situation occurs in nature, as in the heat transfer at the surface of a body of water. Several examples of engineering interest include thermal effects in buildings and electronic equipment, mass-transfer effects in chemical processes that involve liquid-phase contacting, and in electrochemical processes, which inherently involve concentration gradients extending into solution from a solid boundary.

Several researchers have used electrochemical techniques to effect a density gradient at an electrode and monitor the resulting mass transfer. The earliest investigations (Wagner (1949), Wilke, Eisenberg, and Tobias (1953)), and Ibl and Muller (1958), involved determination of free-convection mass transfer at vertical electrodes. Fenech and Tobias (1960) deposited copper at limiting current from acid copper sulphate solutions onto a horizontal cathode facing upward. Depletion of the copper ion from the solution near the electrode resulted in an unstable density gradient. The buoyancy-affected mass-transfer distribution was measured using a sectioned electrode. The mass-transfer distribution could also be evaluated directly from the patterns in the electrodeposit. Boeffard (1966) extended this work using the ferri-ferrocyanide redox couple to measure the mass-transfer limited current to a nickel

cathode in various orientations. Ward and Le Blanc (1984) used the ferric/ferrous couple in chloride solution to effect a density gradient between two closely-spaced electrodes. They repeated the classic Bénard-Rayleigh stability problem by imposing a current (flux) step and monitoring the potential. At very low current densities, the potential gives a direct measure of the ratio of concentrations of Fe^{+3} to Fe^{+2} at the electrodes, from which they could estimate the difference in solution density between the two electrodes. They found the critical Rayleigh number to be 1350 ± 300. Dees and Tobias (1986) used the micro-mosaic electrode to study buoyancy-induced mass transfer at a horizontal cathode facing upward. They observed both chaotic and regular fluctuations in the mass-transfer limited current to the electrode, sometimes occurring simultaneously on different parts of the electrode. They also demonstrated that, while the current to a single electrode element (of area 0.01 mm^2) oscillated about an average value with a peak-to-peak amplitude as large as 83% of the average value, the current to the total electrode area (0.25 cm^2) varied by only about 3%. Apparently, the current oscillations are averaged over a large area.

McLarnon, Muller, and Tobias (1982) used electrochemical and optical techniques in the study of combined free and forced convection. They deposited copper from unsupported $CuSO_4$ and used interferometry to measure the resulting concentration profile.

The above investigators have demonstrated the usefulness of electrochemical techniques for inducing density-driven flows as well as for monitoring the resulting mass transfer. The advantage of the electrochemical technique over the more-traditional thermal method of generating a density gradient is that, by controlling the surface condition electrically, a step change in surface concentration can be effected uniformly and rapidly. The mass-transfer rate to the surface is monitored as the resulting current. This electrochemical detection of the onset of convection by

monitoring the Sherwood number is more precise than flow visualization techniques; the latter cannot discern the initial stages of convection.

The objective of this work is to demonstrate the applicability of electrochemical techniques for the study of a classic Bénard-Rayleigh stability problem with spatial resolution of 100 μm on the monitoring surface. This spatial resolution is attained using a micro-mosaic electrode, which is designed to simulate a continuous surface. Fabricated on a 7.62-cm silicon wafer, it comprises a 10 x 10 array of 98-μm square, electrically-isolated, platinum segments on 100-μm centers. The problem we consider is the mass-transfer analog to the Bénard-Rayleigh problem of a fluid contained in a deep cell whose lower surface is heated impulsively to a constant temperature. A potential step is imposed, resulting in limiting current for the reduction of an indicator ion; the concentration of this species instantaneously becomes zero at the electrode. As a consequence of the ionic species transport by diffusion and migration, the fluid density near the electrode surface is less than that of the fluid above. The problem is analyzed in terms of a Rayleigh number based on the penetration depth of the density profile, and one based on that of the reactant ion concentration profile. We investigate the effects of size and sensitivity of the sensing element on the critical Rayleigh number.

Stability of Impulsively-Heated Fluids

Two different approaches were followed in the early theoretical work on the stability of fluids with a time-dependent density profile (reviewed by Homsy (1973) and Jhaveri and Homsy (1982)). The first workers in this area (Lick, 1965; Currie, 1967) assumed that the disturbance grows much faster than the evolving diffusive profile, so that one can examine the marginal stability of the evolving base state at a

given time. Their approach has been criticized in the literature and is not always valid; this "quasi-steady state" assumption is common in engineering practice, however, and should be used subject to scaling arguments which can demonstrate its applicability. For the case of a sudden change in surface concentration (or temperature), the parameter that should be examined is the Schmidt (or Prandtl) number, the ratio of momentum diffusivity to mass (or thermal) diffusivity. One would not expect the quasi-steady state assumption to be valid for low values of the Schmidt number. In the case of a time-dependent surface condition, one would also not expect this type of analysis to be valid for high rates of surface heating. After extensive comparison of his own experimental data to the early theories, Davenport (1972) concluded that the problem with the quasi-steady state models is not with the quasi-steady state assumption itself, but that a destabilizing influence had been erroneously attributed to the bulk fluid. (For relatively deep pools, $\alpha t / h^2 < 0.1$, Currie's model predictions were a factor of 40 below Davenport's experimental results, even for high Prandtl number.)

The second early theoretical approach is that first used by Foster (1965a, 1968) and followed by several others (Elder (1968), Mahler *et al.* (1968), Mahler and Schechter (1970), and Gresho and Sani (1971)). In this approach the linear stability equations are integrated numerically and the growth rate of an initial velocity disturbance is followed in time. The onset time is determined as the time at which the disturbance has grown to a given amplification of the initial disturbance. The main objection to this approach is that the linearized equations may not be valid during the growth of the disturbance. In addition, the initial disturbance itself and the amplification factor at which one would presume that convection could be observed are somewhat arbitrary. Foster (1968) presented his results in terms of the times to achieve disturbance amplifications of 10 and 10^8. Gresho and Sani (1971) used an

amplification factor of 1000.

In a recent study, Jhaveri and Homsy (1980, 1982) report a rigorous stability analysis of the problem using the method of energy, with thermodynamic fluctuations as the disturbances. Their stability analysis was conducted for a step change of temperature, and also for a linear change, at a free surface with a Prandtl number of 7. Their results are presented in terms of a time-dependent, critical Rayleigh number Ra_t, which is the Rayleigh number based on total fluid depth multiplied by the dimensionless time; the total depth is removed from the problem with this scaling, and the Rayleigh number is based on a nominal penetration depth δ, where $\delta = \sqrt{\alpha t}$. The time of onset of convection is defined as the time at which the thermal flux, or Nusselt number Nu, deviates from convection-free behavior by a given percentage. For a Prandtl number of 7, they found that the time-dependent Rayleigh number does not vary significantly if the Nusselt number deviation criterion is changed over a range of 1 to 10%. This result implies that the disturbance grows quickly relative to the evolution of the diffusive profile. Comparison of Jhaveri and Homsy's results at Pr = 7, for a step change at a free surface, to Foster's 1968 analysis shows that Jhaveri and Homsy's result of $Ra_t = 349$ (Nu variation of 5%) lies between Foster's limits of 61 (amplification = 10) and 630 (amplification = 10^8). (Jhaveri and Homsy's Ra_t corresponds to Foster's $t_c^{3/2}$.)

The early experimental investigations of this problem involved thermal studies (Spangenberg and Rowland (1961), Foster (1965b)), typically using evaporative cooling of water, for which the Prandlt number is approximately 7. In these experiments, neither surface temperature nor thermal flux is exactly constant; the surface temperature and evaporation rate are governed by the coupled mass and energy transfer at the surface. This type of experiment is also quite sensitive to trace impurities which affect the surface tension and hence the rigidity of the surface. How dramatic this

effect can be for water was shown theoretically by Berg and Acrivos (1965), who found that trace contamination, as low as 1% of that required to form a close-packed monolayer, should stabilize a water layer up to a depth of 1 cm. The most important result from the early experiments with water is that, for a deep cell, $\delta/h < 0.3$, the critical time for onset of convection is independent of total fluid depth.

The absorption of an inert gas at a free surface overcomes some of the difficulties associated with evaporative cooling. Plevan and Quinn (1966), Blair and Quinn (1969), and Mahler and Schechter (1970) used this technique to investigate the onset of buoyancy-induced convection. In a gas absorption experiment, the surface boundary condition can be altered by changing the pressure of the absorbing gas above the liquid. The concentration of dissolved gas at the surface is directly proportional to the gas pressure; the constant of proportionality is the Henry's constant. A sudden change in surface concentration can be effected, and an analytic solution is obtained for the concentration profile. The density of the fluid is linearly dependent on the dissolved gas concentration over a wide range, so that the density profile can be derived as well. With this technique, the surface properties will be sensitive to the presence of trace impurities of surface-active agents in the fluid; the effect can be minimized (or maximized), however, through the choice of the gas-liquid pairs.

Davenport and King (1974) conducted an extensive series of experiments with fluids covering a wide range of Prandtl numbers (0.7 to 8500). They contained the fluids between two plates and adjusted the heating rate to maintain either a constant lower plate temperature, or one which varied as a prescribed function of time. Results are presented in terms of the Rayleigh number based on the nominal penetration depth described above. They also used a Rayleigh number Ra_l based on the equivalent linear-segment penetration depth originally proposed by Lick (1965),

$$l = 2 \int_0^\infty \frac{(T - T^\infty)}{(T^0 - T^\infty)}\, dy \quad , \tag{1}$$

which, for the case of constant surface temperature, is equal to $\frac{2}{\sqrt{\pi}} \sqrt{4\alpha t}$. When Davenport and King compared their results to Foster's model, they found that the apparent amplification factor at convection onset decreases as the Prandtl number increases. Their value of Ra_l was independent of Prandtl number, and of total fluid depth, and was found to be approximately 1700, the critical Rayleigh number for the classic time-independent problem of a fluid contained between two rigid walls (Jeffreys, 1928).

The experimental procedure used in this study is closely related to the gas absorption experiments described above. In this study, an electrochemical technique is used to effect the change in surface concentration uniformly and rapidly. Our treatment of experimental results most closely parallels that of Davenport and King. We use a Rayleigh number based on penetration depth of the reacting species. The multi-component species problem that we encounter results in a density profile with a slight maximum so that we will also use a penetration depth based on the density profile. The Schmidt number is high for the present case ($\sim$ 2300, typical of aqueous solutions), so that the quasi-steady state analysis should be applicable.

Experimental

The micro-mosaic electrode used in this study was conceived by Dees and Tobias (1982) in this laboratory and was originally designed in a collaborative effort with the Hewlett-Packard Company. The design was modified for this investigation, and the electrodes were fabricated using integrated-circuit technology at Hewlett Packard Laboratories, and later at AT&T Bell Laboratories. The electrode, shown in

Figure 1, is fabricated on a 7.62-cm silicon wafer. The active area consists of a 5-mm platinum square. The center 1-mm square of the active area comprises a 10×10 array of 98-μm square, platinum segments on 100-μm centers; the remaining part of the active area acts as a "buffer" segment to eliminate edge effects in the center region. An enlargement of the center section is shown in Figure 2. The electrode simulates a continuous surface which contains one hundred electrically-isolated electrode elements.

The electrode is housed in a plexiglass cell into which are built two platinum counter electrodes and a reference-electrode capillary. A data acquisition system developed by Dees (1983) is used to monitor the current to each of the electrode segments at rates from 1.25 to 10.0 KHz. Dees and Tobias (1982, 1986) give a detailed description of the electrode fabrication and data acquisition system.

We impose a potential step into the potential region of limiting current for the reduction of Fe^{+3} to Fe^{+2} from 0.0484 M $Fe_2(SO_4)_3$ in 0.5 M H_2SO_4. The current responses at the electrode segments are monitored and stored digitally.

Care was taken to ensure that the solution concentration was uniform and that the solution was quiescent prior to the start of an experiment. All cell parts were cleaned with distilled, deionized water and methanol. Reagent grade chemicals were used. Surface-tension driven flows were not a concern in our experiments, the electrode itself providing a rigid surface, so ultra-clean conditions were not a necessity. The cell temperature was monitored, but not controlled, in the experiments. Thermal effects due to heat generation are insignificant in our system. Even if all of the power dissipated in the system were released at the electrode surface, the density difference resulting from thermal effects would be less than 1% of that resulting from mass-transfer effects.

Analysis of the Base-State Profile

The description of a multi-component, electrochemical system is necessarily more complex than that of a thermal system. This analysis is conducted to obtain an estimate for the surface concentration of each of the ions in solution. From the surface concentrations, we can calculate the solution density at the electrode surface. We also obtain the concentration and density profiles through the solution and the flux at the surface (current) as a function of time.

A potential step into the limiting-current regime involves a sudden change in electrode potential to a value at which the rate of reaction is limited only by the mass transfer of the reactant ion to the surface. This potential step results in an instantaneous drop in the concentration of the reactant ion Fe^{+3} at the electrode. At the same time, the reaction product Fe^{+2} starts to build up at the electrode. In the absence of convection, the region of depleted Fe^{+3} and enhanced Fe^{+2} extends farther and farther into the solution with time, increasing the resistance for mass transport to the electrode surface. The concentrations of the major supporting-electrolyte species, H^{+} and SO_4^{-2}, are governed by diffusion and by migration in the electric field in such a way that solution electroneutrality is maintained.

The equation governing the one-dimensional mass transport of species i due to diffusion and migration is (Newman, 1973)

$$\frac{\partial c_i}{\partial t} = D_i \frac{\partial^2 c_i}{\partial y^2} + z_i u_i F \frac{\partial \left(c_i \frac{\partial \phi}{\partial y} \right)}{\partial y} \quad . \tag{2}$$

u_i is the ionic mobility of species i and can be related, for solutions dilute in species i, to the diffusion coefficient by the Nernst-Einstein relation,

$$u_i = \frac{D_i}{RT} \quad . \tag{3}$$

The condition of electroneutrality is the other equation required to solve for the species concentrations and the potential, ϕ.

$$\sum_i^4 z_i c_i = 0 \tag{4}$$

Initially, each species is at its bulk concentration,

$$c_i(0,y) = c_i^{\infty} \quad , \tag{5}$$

The boundary conditions at the electrode surface are

$$c_{Fe^{+3}}(t,0) = 0 \tag{6}$$

and

$$D_i \left(\frac{\partial c_i}{\partial y} + \frac{z_i F}{RT} c_i \frac{\partial \phi}{\partial y} \right) = \frac{s_i}{s_R} D_R \left(\frac{\partial c_R}{\partial y} + \frac{z_R F}{RT} c_R \frac{\partial \phi}{\partial y} \right) \tag{7}$$

where R refers to the reactant species Fe^{+3}, and s_i is the stoichiometric coefficient of species i when the electrode reaction is written as

$$\sum_i s_i M_i \rightarrow n e^- \quad . \tag{8}$$

For a nonreacting species, s_i is zero. The electrode reaction in our case is

$$- Fe^{+3} + Fe^{+2} \rightarrow e^- \quad . \tag{9}$$

The net flux of each of the non-reacting ions, H^+ and SO_4^{-2}, is zero at the electrode surface. Far away from the electrode, the species concentrations are equal to their initial bulk values,

$$c_i(t,\infty) = c_i^{\infty} \quad . \tag{10}$$

The above set of equations describes the species transport in a quiescent solution. The equations may be transformed to ordinary differential equations using the similarity variable,

$$\eta = \frac{y}{\sqrt{4D_R\, t}} \quad . \tag{11}$$

The transformed equations and boundary conditions are given in the Appendix. The set of transformed, coupled, ordinary differential equations was solved using the Galerkin finite-element method with linear basis functions and weighting functions.† The mesh was refined until the solution values remained unchanged to 5 significant figures. One thousand equally-spaced elements were used over a range of η from 0 to 4. Because the equations are nonlinear, a Newton-Raphson iterative technique was used. An IMSL Library subroutine (1982) was used to solve the linearized equations at each iteration. The solution was considered to be converged when the root mean square of the corrections to the previous iteration's values was less than 10^{-10}. The number of iterations required to acheive convergence depends on the initial guess, but usually no more than four were necessary, consuming 16 seconds of CPU time per iteration on a Vax 8600 computer.

The current is proportional to the derivative of the concentration of reactant ion at $\eta = 0$, which is a function of the diffusion coefficients and bulk concentrations of all of the ions:

$$i = \frac{nFD_R}{s_R\sqrt{4D_R\, t}} \left(\frac{dc_R}{d\,\eta}\right)_{(\eta\,=\,0)} \quad . \tag{12}$$

† A Fortran program that solves the same set of coupled equations using a finite-difference method can be found in Newman (1973, pp. 423-24)

The solution to the above equations reduces to the Cottrell equation (Bard and Faulkner, 1980) for the current resulting from a potential step when the reactant is in an infinitely-supported solution. In such a case, transport of the reactant ion by migration is negligible, and $\left(\frac{dc_R}{d\eta}\right)_{(\eta=0)} = \frac{2c_R^{\infty}}{\sqrt{\pi}}$.

The reason for a density difference across the diffusion layer can best be seen by writing the electrode reaction as

$$Fe_2(SO_4)_3 + 2e^- \rightarrow 2FeSO_4 + SO_4^{-2} \quad . \tag{13}$$

SO_4^{-2} is transported away from the electrode and H^+ is transported to the electrode, maintaining electroneutrality. The net result is that the solution near the electrode is less dense than that in the bulk. The extent to which each of these two ions accumulates or depletes at the electrode surface is a complex function of the diffusion coefficients and charges of *all* ionic species present in the electrolyte.

The density profile is obtained from the concentration profiles using

$$\rho = \rho^{\infty} + \rho^{\infty} \sum_i \alpha_i \, (c_i - c_i^{\infty}) \tag{14}$$

where α_i is the densification coefficient for species i. Since ionic species may occur only in the form of neutral pairs, the densification coefficient of any one of the ionic species may be set to zero without loss of generality. For convenience, SO_4^{-2} is chosen because it is common to all of the neutral pairs; the densification effect of SO_4^{-2} is then included with that of the associated cation. Since the major electrolyte species is H_2SO_4, its densification coefficient was fitted by linearizing H_2SO_4 solution density data (Weast, 1977) near the bulk concentration. The densification coefficient for Fe^{+3} was estimated in two ways: (1) by fitting literature density information for pure $Fe_2(SO_4)_3$ solutions (Perry and Chilton, 1973), and (2) by fitting our own

density measurements for the $Fe_2(SO_4)_3/H_2SO_4$ system. These two values differed by 4.9% An estimate for $\alpha_{Fe^{+2}}$ was obtained using literature data (Perry and Chilton, 1973) for pure $FeSO_4$ solution densities.

The diffusion coefficients for H^+ and SO_4^{-2} were taken from literature data (Newman, 1973, p.230). The diffusion coefficient for Fe^{+3} was obtained from the initial part of the potential step experiment before convection onset (Eq. (10)). The product Fe^{+2} diffusion coefficient was calculated from that of Fe^{+3} on the basis of published values (Dean, 1979) of the equivalent ionic conductances of the two ions.

Results and Discussion

Our main objective in solving the model presented in the previous section is to calculate the concentration profiles and density profile for the base state. Had we been depositing a metal from an unsupported electrolyte, rather than using a redox reaction, the equations would reduce to the thermal equations for which an analytic solution is available. The advantage of the redox system is that there are no surface-roughening effects, which commonly occur in metal deposition.

The concentration profile of the reactant ion is shown in Figure 3. The equivalent, linear-segment penetration depth l_c was calculated from the mass-transfer analog to Eq. (1),

$$l_c = 2 \int_0^\infty \frac{(c_R - c_R^\infty)}{(c_R^0 - c_R^\infty)} \, dy \quad . \tag{15}$$

l_c was found to correspond to a dimensionless distance η_c of 1.1417. The density profile is calculated from the ion concentration profiles according to Eq. (14) and is shown in Figure 4. There is a slight density maximum in the density profile (also

noted by Selman and Newman, 1971), which occurs at η_m of 1.556. Surface and bulk concentrations and the parameters used in the model are given in Table 1.

An example of the current response of a single segment to a potential step into limiting current is given in Figure 5. The time to onset of convection is more clearly seen when the same data are plotted versus the inverse square root of time, as suggested by the similarity variable. This curve, shown in Figure 6, is typical of what is obtained for most of the working segments. There are, however, some segments, each of which was adjacent to a non-working segment, for which the inverse-square-root-of-time plot exhibits significant curvature throughout the period before convection starts. An example is given in Figure 7. Although the onset of convection is still observable, these segments were not used in the determination of the critical Rayleigh number. Only those segments which showed no appreciable curvature and had straight-line correlation coefficients greater than 0.999 were used. Data from 55 seg-

Table 1. Model Input Parameters and Surface Concentrations

Species	$D_i \times 10^6$ $\left(\frac{cm^2}{sec}\right)$	α_i $\left(\frac{cm^3}{mol}\right)$	$c_i^{\infty} \times 10^3$ $\left(\frac{mol}{cm^3}\right)$	$c_i^{0} \times 10^3$ $\left(\frac{mol}{cm^3}\right)$
H^+	93.12	30.1	1.0	1.0426
SO_4^{-2}	10.65	0.0	0.6454	0.6147
Fe^{+2}	5.135	126.6	0.0	0.0934
Fe^{+3}	4.351	168.0	0.0969	0.0

ments were deemed acceptable.

The diffusion coefficient of Fe^{+3} was calculated from data obtained from each of the 55 segments. The average value is 4.335×10^{-6} cm ^{2}/sec, with a standard deviation of 0.32×10^{-6} cm ^{2}/sec. The total current response for all 55 segments is plotted versus time in Figure 8, and versus the inverse square root of time in Figure 9. The diffusion coefficient for Fe^{+3} from Figure 9 is 4.351×10^{-6} cm ^{2}/sec. The correlation coefficient for straight-line behavior up to the first marker is greater than 0.9999.

The critical Rayleigh number is

$$Ra_l = \frac{\Delta\rho \; g l_c^{\,3}}{\rho^{\infty} \nu D_R} \quad , \tag{16}$$

where l_c , calculated from the model results (Eq. (15)), is

$$l_c = 1.1417 \sqrt{4 D_R \, t_c} \quad . \tag{17}$$

$\Delta\rho/\rho^{\infty}$ is calculated from

$$\frac{\Delta\rho}{\rho^{\infty}} = \sum_i \alpha_i \; (\; c_i{}^0 - c_i{}^{\infty} \;) \quad . \tag{18}$$

t_c was identified as the time when a deviation greater than 5% occurred in the current (Sherwood number) versus inverse-square-root-of-time plot. The choice of a 5% deviation criterion is somewhat arbitrary; however, Jhaveri and Homsy (1982) predicted that the critical Rayleigh number should be fairly insensitive to this criterion in the range between 1 and 10%.

The critical time for onset of convection was determined for each of the 55 segments. The average value is 30.8 seconds, with a standard deviation of 6.6 seconds. The corresponding Rayleigh number is 1330, and l_c is 264 μm. The critical time

determined from the curve of the sum of all of the segments (Figures 8,9) is 33.3 seconds, which gives a Ra_l of 1497 and l_c of 275 μm.

Upon repeating the experiments using different electrodes, the measured onset times were 32.5, 32.9, and 34.1 seconds; the average value for the four runs is thus 33.2 seconds with a maximum deviation of 1.9 seconds. Blair and Quinn (1969) obtained an average onset time of 27 seconds with a range of 24 to 30 seconds in a typical set of gas-absorption experiments. The good reproducibility we observed is an indication of the precision of the electrochemical technique.

The appropriate comparison of our data to theory would involve consideration of the model of Jhaveri and Homsy (1982); however, they did not analyze the problem with a rigid surface or for Prandtl number other than 7. The most direct comparison to theory that we can attempt is to consider Foster's (1968) limiting values obtained using amplification theory. Our Ra_l values fall within Foster's range for $Pr \rightarrow \infty$. He reports Ra_l of approximately 900 for an amplification factor of 10 and approximately 5000 for an amplification factor of 10^8. Davenport and King (1974) found that, with increasing Pr, their experimentally-determined values of Ra_l decreased to an amplification factor of 10 according to Foster's theory.

The Effect of a Density Maximum

The effect of a density maximum, which occurs in the multi-component diffusion problem encountered here, was first treated by Veronis (1963), in connection with the problem of thermal gradients in water near 3.98 ° C confined between two boundaries. The topic remains a subject of current investigation (see Blake *et al.*, 1984, and references therein). The problem of determining the relevant length for such a system has not been resolved (see, for example, Merker *et al.*, 1979), and is even more complex for the semi-infinite system which we encounter. The linear-

segment penetration depth was originally proposed (Lick, 1965) to represent an equivalent integrated buoyant force,

$$l = 2 \int_0^\infty \frac{(\rho - \rho^\infty)}{(\rho^0 - \rho^\infty)}\, dy \quad , \tag{19}$$

and reduces to Eq. (1) when density can be treated as a linear function of temperature. Similarly, it would reduce to Eq. (15) if density were a linear function of c_R. The use of Eq. (19) when there is a density maximum results in the maximum contributing an artificial stabilization by *decreasing* l. For this case it is more appropriate to use a linear segment profile from ρ^0 to ρ^∞ that represents the equivalent destabilizing buoyant force *below* the position of the density maximum y_m,

$$l_m = 2 \int_0^{y_m} \frac{(\rho - \rho^m)}{(\rho^0 - \rho^\infty)}\, dy \quad . \tag{20}$$

For the system treated here,

$$l_m = 0.9530 \sqrt{4 D_R\, t} \quad , \tag{21}$$

which is 16% lower than l_c. There is no *a priori* way to relate these two lengths. l_c is a function of the diffusion coefficients, charges, and bulk concentrations of all of the species, while l_m is a function of all of the above *and* the densification coefficients. The critical Rayleigh number $\mathrm{Ra_m}$ based on l_m is 774 for the single-electrode data and 871 using the entire electrode data.

There has long been some uncertainty regarding the effect of the sensitivity of the monitoring technique on the critical Rayleigh number determined. With the micro-mosaic electrode we can conveniently investigate two effects: (1) the size of the sensing element relative to the that of the convective disturbance and (2) the effect of the chosen deviation criterion.

The Effect of Size of the Sensing Element

Single electrode segments are 100 μm square. According to traditional stability theory, the wavelength of the disturbance is on the order of twice the characteristic length, which for our case is l_c. Thus our sensing elements are significantly smaller than the wavelength of the disturbance. Together they form a cluster (1 mm square) on the same order as the disturbance, which is in turn surrounded by a larger "buffer" section. The effects of averaging on a large scale can be seen by simply comparing the time of the onset of convection for the individual segments to that for the larger cluster of segments, 30.8 versus 33.3 seconds. The longer time required until the onset of convection can be discernable for the larger cluster is the result of mass-transfer fluctuations being averaged on the larger scale.

Close inspection of Figure 5, the response of a single segment, and Figure 8, the response of the entire electrode, reveals another interesting point in regard to the effect of size of the sensing element. Let us for the moment relax the 5% deviation criterion and consider instead the time until a *major* enhancement of the mass-transfer rate due to convection is established. This significant enhancement is the onset criterion one would probably detect in gas absorption experiments at a free surface without a very sensitive monitoring instrument. That the deviation from base-state behavior, according to our 5% criterion, significantly precedes any *major* enhancement in the current for the entire electrode can be seen in Figure 8. By contrast, the response for a single electrode element, shown in Figure 5, exhibits a significant increase in current immediately following the first deviation and much sooner than the entire electrode. If the Rayleigh number were based on the beginning of the sharp increase in current to the entire electrode ($\sim$ 50 seconds), it would be a factor of approximately 1.9 higher than the one determined from the 5% criterion we used. For the single-electrode data, the Rayleigh number would increase considerably

less, by a factor of 1.3.

The Effect of the Chosen Deviation Criterion

The effect of varying the Sherwood number deviation criterion from 5 to 10% was investigated using the total current for all of the segments, shown in Figure 9. Over this range of onset criteria, the critical time varied from 33.3 seconds (at 5%) to 37.6 seconds (at 10%), an increase of 13%. The consequent increase in the calculated Ra_l is 20%. Jhaveri and Homsy (1982) predict that for Pr = 7 at a free surface, the measured Ra_l would increase by only 4% if the flux criterion is changed from 5 to 10%. Since we have a very high Schmidt number (2300), we might expect less of an effect of the onset criterion than predicted by Jhaveri and Homsy. Inspection of Figure 8 shows a definite departure from the base-state behavior at the marker for 5% deviation; however, the current response is still somewhat flat before the convection dominates and a very strong increase is seen. If we consider the current response of a single segment, we might see a sharper increase (or decrease) at convection onset than in the case of the sum of all the segments, where some averaging will undoubtedly take place. Figure 10 illustrates the current response for a segment showing a sharp negative deviation from the base-state behavior. The first marker (to the right in the figure) shows the last point for the calculation of the slope and correlation coefficient. The second marker (to the left) shows the point of 5% deviation. The time of convection onset for this curve is 39.8 seconds for a 5% deviation and 43.1 seconds for a 10% deviation, an 8.3% increase. The corresponding effect on the Rayleigh number is an increase of 12.7%, closer to the predicted value, but still significantly higher. One reason why we might not expect a close comparison between our result and Jhaveri and Homsy's model is that the model was established for a free surface condition, which means that there is no shear stress at that surface to retard flow development.

It is of particular interest to consider the temporal and spatial variation of the direction of the change in mass transfer at the onset of convection. In the development of a cellular motion, we might expect to see areas where the initial deviation from the base-state current-time behavior is an enhanced transport rate and others where the rate is lowered. Indeed this was the case. About two-thirds of the electrode surface showed a positive deviation, while a negative deviation occurred on the rest. The current to a segment showing a positive deviation is given in Figure 11, and that for a segment 100 microns away showing a negative deviation is given in Figure 12. The segment between these two, shown in Figure 13, underwent two slight negative deviations followed finally by a large increase in the current. The segmented area of the micro-mosaic electrode is too small to completely surround the entire area of segments showing the same type deviation. This distribution of deviations was not investigated in repeated experiments; however, all runs showed an overall *increase* in mass-transfer rate at the time of convection onset.

Conclusions

The use of a micro-mosaic electrode with an electrochemical redox system has been demonstrated in a study of the Bénard-Rayleigh problem of onset of convection in a fluid with a time-dependent density profile contained in a deep cell. The electrochemical technique offers several advantages over thermal techniques, the most important one being the precise control of the surface condition. The well-controlled experiment lends itself to a thorough analysis of the time-dependent base state, the case of diffusion and migration into a semi-infinite column of electrolyte. In addition, the electrode serves as the monitoring device, allowing a precise detection of the onset of convection, the criterion for which is a percentage deviation of the Sherwood number

(current) from base-state behavior.

The critical Rayleigh number Ra_l for the problem of onset of convection at a rigid, conducting boundary, due to a step change in the surface condition, was found to be approximately 1350, based on the equivalent, linear-segment concentration profile and using a deviation criterion of 5% of the Sherwood number. For the redox system employed here, we calculate a maximum in the density profile. The relevant length for the equivalent, linear-segment density profile, based on an equivalent destabilizing buoyant force below the density maximum, is 16% lower than that for the concentration profile of the reactant. The critical Rayleigh number Ra_m based on this length is approximately 800.

At sensing elements much smaller than the wavelength of the disturbance, a sharp increase (or decrease) in mass-transfer rate occurs immediately after the first deviation from convection-free behavior. Over a larger area, some averaging takes place and a significant enhancement of the mass-transfer rate does not occur until tens of seconds after the first deviation in the mass-transfer rate is detected. For these reasons the single-segment data are less sensitive to the choice of the criterion that defines the time of deviation from convection-free behavior than are the data obtained from the entire electrode. Ra_l for single segments increased approximately 13% when the onset criterion was raised from a 5 to 10% deviation, while Ra_l derived from the entire electrode increased by 20%.

Acknowledgment

The authors are most grateful for the generous contribution of both time and effort on the part of Hewlett-Packard Company and AT&T Bell Laboratories in the design and fabrication of the micro-mosaic electrodes. This work was supported by

the Assistant Secretary of Conservation and Renewable Energy, Office of Energy Systems Research, Energy Storage Division of the U.S. Department of Energy under Contract DE-AC03-76SF00098. Gina Whitney received fellowship support from the National Science Foundation and the Exxon Education Foundation.

References

Bard, A. J., and Faulkner, L. R., 1980, *Electrochemical Methods*, John Wiley & Sons, New York, pp. 142-144.

Berg, J. C., and Acrivos, A., 1965, "The Effect of Surface Active Agents on Convection Cells Induced by Surfece Tension," *Chemical Engineering Science*," Vol. 20, pp. 737-745.

Blair, L. M., and Quinn, J. A., 1969, "The Onset of Cellular Convection in a Fluid Layer with Time-Dependent Density Gradients," *Journal of Fluid Mechanics*, Vol. 36, part 2, pp. 385-400.

Blake, K. R., Poulikakos, D., and Bejan, A., 1984, "Natural Convection near 4 °C in a Horizontal Water Layer Heated from Below," *The Physics of Fluids*, Vol. 27, pp. 2608-2616.

Boeffard, A. J.-L., 1966, *Ionic Mass Transport by Free Convection in a Redox System*, M. S. Thesis, University of California, Berkeley. (Also Lawrence Radiation Laboratory Report No. UCRL-16624)

Currie, I. G., 1967, "The Effect of Heating Rate on the Stability of Stationary Fluids," *Journal of Fluid Mechanics*, Vol. 29, part2, pp. 337-347.

Davenport, I. F., 1972, *The Initiation of Natural Convection Caused by Time-Dependent Profiles*, Ph. D. Thesis, University of California, Berkeley. (Also Lawrence Berkeley Laboratory Report No. LBL-660)

Davenport, I. F. and King, C. J., 1974, "The Onset of Convection from Time-Dependent Profiles," *International Journal of Heat and Mass Transfer*, Vol. 17, pp. 69-76.

Dean, J. A., Ed., 1979, *Lange's Handbook of Chemistry, Twelfth Edition*, McGraw-Hill Book Company, New York, New York, p. **6**-34.

Dees, D. W., 1983, *Mass Transfer at Gas-Evolving Surfaces in Electrolysis*, Ph. D. Thesis, University of California, Berkeley. (Also Lawrence Berkeley Laboratory Report No. LBL-16176)

Dees, D. W., and Tobias, C. W., 1982, "A Novel Micro-Mosaic Electrode for the

Study of Transport Phenomena at Gas-Evolving Electrodes," *Extended Abstracts of the 33rd International Society of Electrochemistry Meeting*, Vol. I, pp. 456-458.

Dees, D. W., and Tobias, C. W., 1986, "Experimental Studies of Free-Convection Mass Transfer to a Horizontal Surface with a Micro-Mosaic Electrode," in press, *Journal of the Electrochemical Society*, Vol. 133, pp. 000-000.

Elder, J. W., 1968, "The Unstable Thermal Interface," *Journal of Fluid Mechanics*, Vol. 32, part 1, pp. 69-96.

Fenech, E. J. and Tobias, C. W., 1960, "Mass Transfer by Free Convection at Horizontal Electrodes," *Electrochimica Acta*, Vol. 2, pp. 311-325.

Foster, T. D., 1965a, "Stability of a Homogeneous Fluid Cooled Uniformly from Above," *The Physics of Fluids*, Vol. 8, pp. 1249-1257.

Foster, T. D., 1965b, "Onset of Convection in a Layer of Fluid Cooled from Above," *The Physics of Fluids*, Vol. 8, pp. 1770-1774.

Foster, T. D., 1968, "Effect of Boundary Conditions on the Onset of Convection," *The Physics of Fluids*, Vol. 11, pp. 1257-1262.

Gresho, P. M. and Sani, R. L., 1971, "The Stability of a Fluid Layer Subjected to a Step Change in Temperature: Transient versus Frozen Time Analyses," *International Journal of Heat and Mass Transfer*, Vol. 14, pp. 207-221.

Homsy, G. M., 1973, "Global Stability of Time-Dependent Flows: Impulsively Heated or Cooled Fluid Layers," *Journal of Fluid Mechanics*, Vol. 60, part 1, pp. 129-139.

Ibl, N. and Muller, R. H., 1958, "Studies of Natural Convection at Vertical electrodes," *Journal of the Electrochemical Society*, Vol. 105, pp. 346-353.

IMSL Inc., 1982, IMSL Library, Edition 9, IMSL, Inc., Houston, Texas.

Jeffreys, H., 1928, "Some Cases of Instability in Fluid Motion," *Proceedings of the Royal Society of London, Series A*, Vol. 118, pp. 195-208.

Jhaveri, B. S. and Homsy, G. M., 1980, "Randomly-Forced Rayleigh- Bénard Convection," *Journal of Fluid Mechanics*, Vol. 98, part 2, pp. 329-348.

Jhaveri, B. S. and Homsy, G. M., 1982, "The Onset of Convection in Fluid Layers Heated Rapidly in a Time-Dependent Manner," *Journal of Fluid Mechanics*, Vol. 114, pp. 251-260.

Lick, W., 1965, "The Instability of a Fluid Layer with Time-Dependent Heating," *Journal of Fluid Mechanics*, Vol. 21, part 3, pp. 565-576.

Mahler, E. G. and Schechter, R. S., 1970, "The Stability of a Fluid Layer with Gas Absorption," *Chemical Engineering Science*, pp. 955-968.

Mahler, E. G., Schechter, R. S., and Wissler, E. H., 1968, "Stability of a Fluid Layer

with Time-Dependent Density Gradients," *The Physics of Fluids*, Vol. 11, pp. 1901-1912.

McLarnon, F. R., Muller, R. H., and Tobias, C. W., 1982, "Interferometric Study of Combined Forced and Natural Convection," *Journal of the Electrochemical Society*, Vol. 129, pp. 2201-2206.

Merker, G. P., Waas, P., and Grigull, U., 1979, "Onset of Convection in a Horizontal Water Layer with Maximum Density Effects," *International Journal of Heat and Mass Transfer*, Vol. 22, pp. 505-515.

Newman, J. S., 1973, *Electrochemical Systems*, Prentice-Hall, Inc., Englewood Cliffs, New Jersey, pp. 355-357.

Perry, R. H. and Chilton, C. H., Eds., 1973, *Chemical Engineers' Handbook, 5th Edition*, McGraw-Hill Book Company, New York, New York, p. 3-75.

Plevan, R. E., and Quinn, J. A., 1966, "The Effect of Monomolecular Films on the Rate of Gas Absorption into a Quiescent Liquid," *The American Institute of Chemical Engineers Journal*, Vol. 12, pp. 894-902.

Selman, J. R., and Newman, J., 1971, "Free Convection Mass Transfer with a Supporting Electrolyte," *Journal of the Electrochemical Society*, Vol. 118, pp. 1070-1078.

Spangenberg, W. G, and Rowland, W. R., 1961, "Convective Circulation in Water of Induced by Evaporative Cooling," *The Physics of Fluids*, Vol. 4, pp. 743-750.

Veronis, G., 1963, "Penetrative Convection," *Astrophysical Journal*, Vol. 137, pp. 641-663.

Wagner, C., 1949, "The Role of Natural Convection in Electrolytic Processes," *Transactions of the Electrochemical Society*, Vol. 95, pp. 161-173.

Ward, W. J., III, and LeBlanc, O. H., Jr., 1984, "Rayleigh-Bénard Convection in an Electrochemical Redox Cell," *Science*, Vol. 225, pp. 1472-1473.

Weast, R. C., Ed., 1977, *CRC Handbook of Chemistry and Physics, 58th Edition*, CRC Press, Inc., West Palm Beach, Florida, p. F-7.

Wilke, C. R., Eisenberg, M., and Tobias, C. W., 1953, "Correlation of Limiting Current under Free Convection Conditions," *Journal of the Electrochemical Society*, Vol. 100, pp. 513-523.

Appendix

The dependent variables in the equation for mass transport by diffusion and migration in a semi-infinite column of electrolyte (Eq. (2)) are made dimensionless as

$$\theta_i = \frac{c_i}{c_R^{\infty}} \tag{A-1}$$

$$\Phi = \frac{\phi F}{RT} \quad . \tag{A-2}$$

Substituting these into Eq. (2) gives

$$\frac{\partial \theta_i}{\partial t} = D_i \frac{\partial^2 \theta_i}{\partial y^2} + z_i D_i \left(\frac{\partial \theta_i}{\partial y} \frac{\partial \Phi}{\partial y} + \theta_i \frac{\partial^2 \Phi}{\partial y^2} \right) \quad . \tag{A-3}$$

Eq (A-3) is transformed to an ordinary differential equation using the similarity variable

$$\eta = \frac{y}{\sqrt{4 D_R t}} \quad , \tag{A-4}$$

and becomes

$$2\eta \frac{d\,\theta_i}{d\,\eta} + \frac{D_i}{D_R} \frac{d^2 \theta_i}{d\,\eta^2} + \frac{D_i}{D_R} z_i \left(\frac{d\,\theta_i}{d\,\eta} \frac{d\,\Phi}{d\,\eta} + \theta_i \frac{d^2 \Phi}{d\,\eta^2} \right) = 0 \quad . \tag{A-5}$$

The boundary conditions at $y = \infty$ and the initial conditions combine to give

$$\theta_i = \frac{c_i^{\infty}}{c_R^{\infty}} \tag{A-6}$$

$$\Phi = 0 \tag{A-7}$$

at $\eta = \infty$. The surface boundary conditions at $\eta = 0$ become

$$\theta_R = 0 \tag{A-8}$$

$$D_i \left(\frac{d\,\theta_i}{d\,\eta} + z_i \theta_i \frac{d\,\Phi}{d\,\eta} \right) = \frac{s_i}{s_R} D_R \left(\frac{d\,\theta_R}{d\,\eta} + z_R \theta_R \frac{d\,\Phi}{d\,\eta} \right) \tag{A-9}$$

The equation of electroneutrality (Eq. (4)) becomes

$$\sum_i^4 z_i \theta_i = 0 \tag{A-10}$$

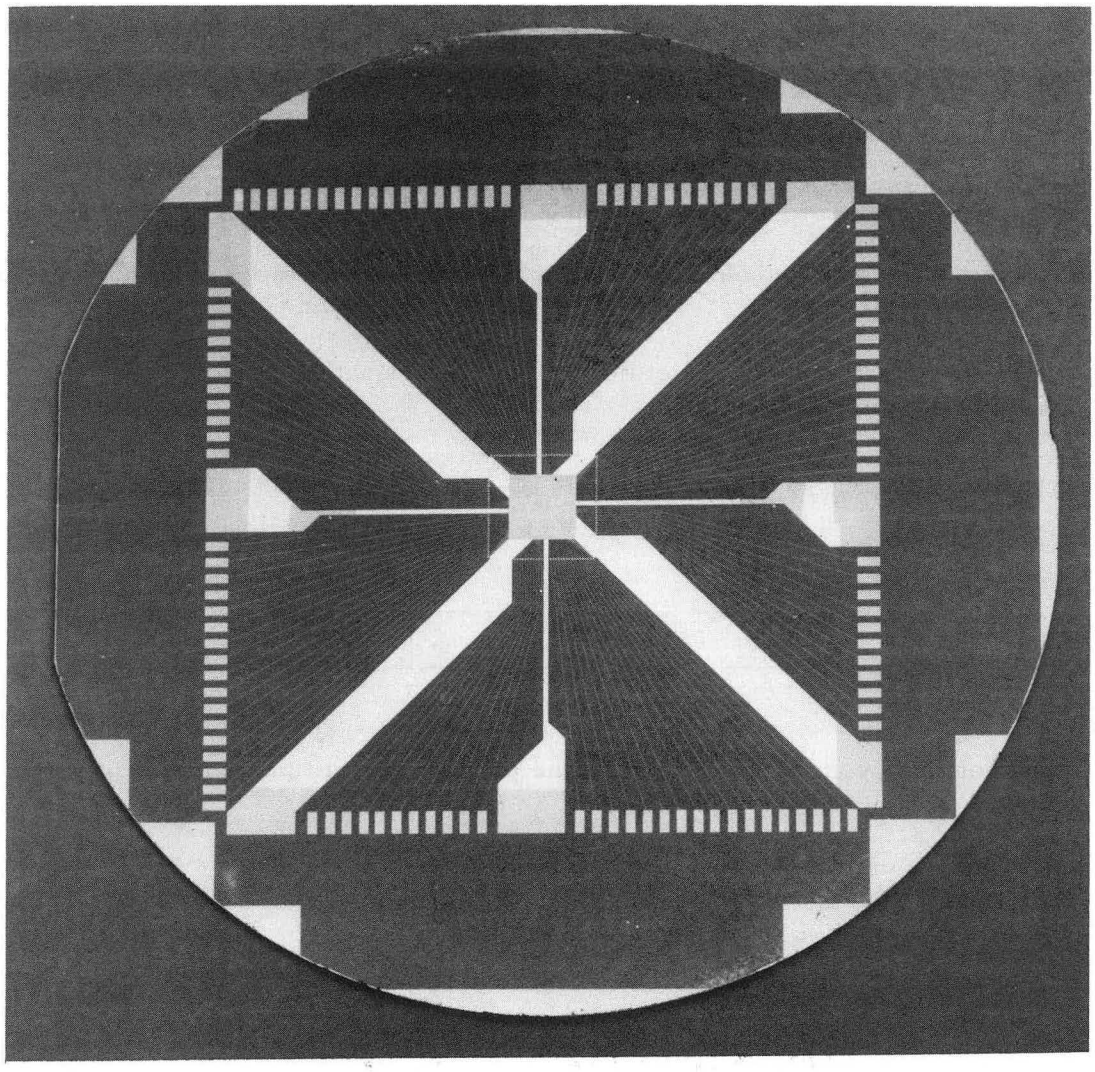

CBB 809-1D993

Figure 1. Micro-mosaic electrode fabricated on a 7.62-cm silicon wafer.

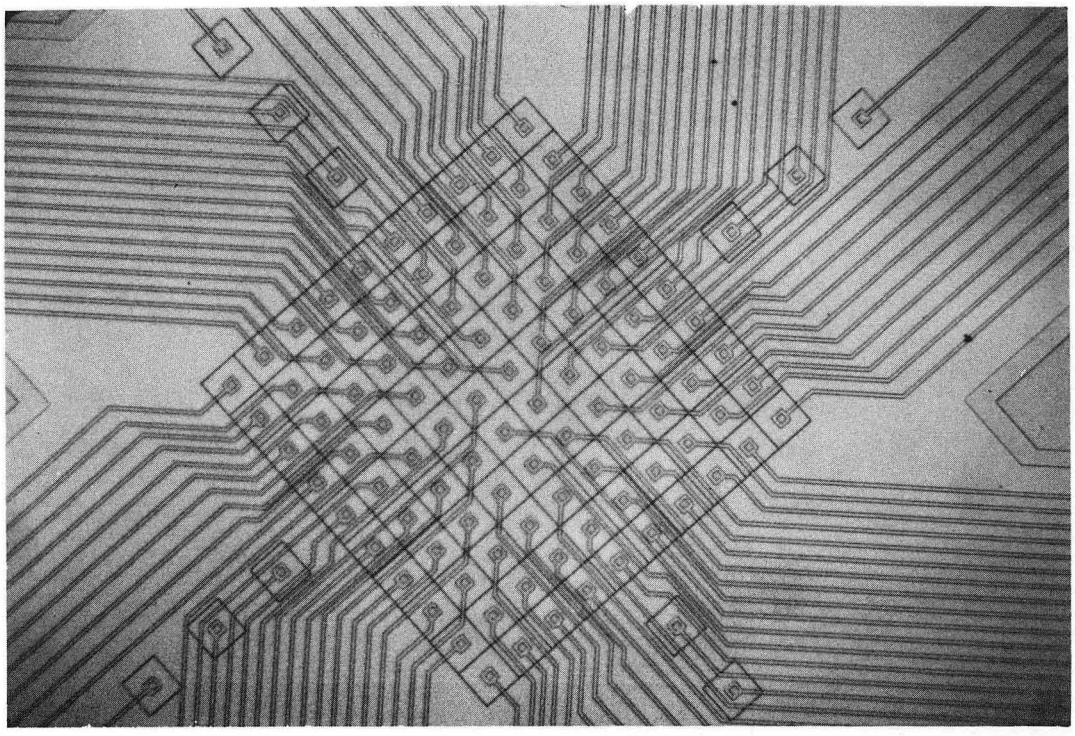

Figure 2. Center segmented portion (1-mm square) of the micro-mosaic electrode. CBB809-11046

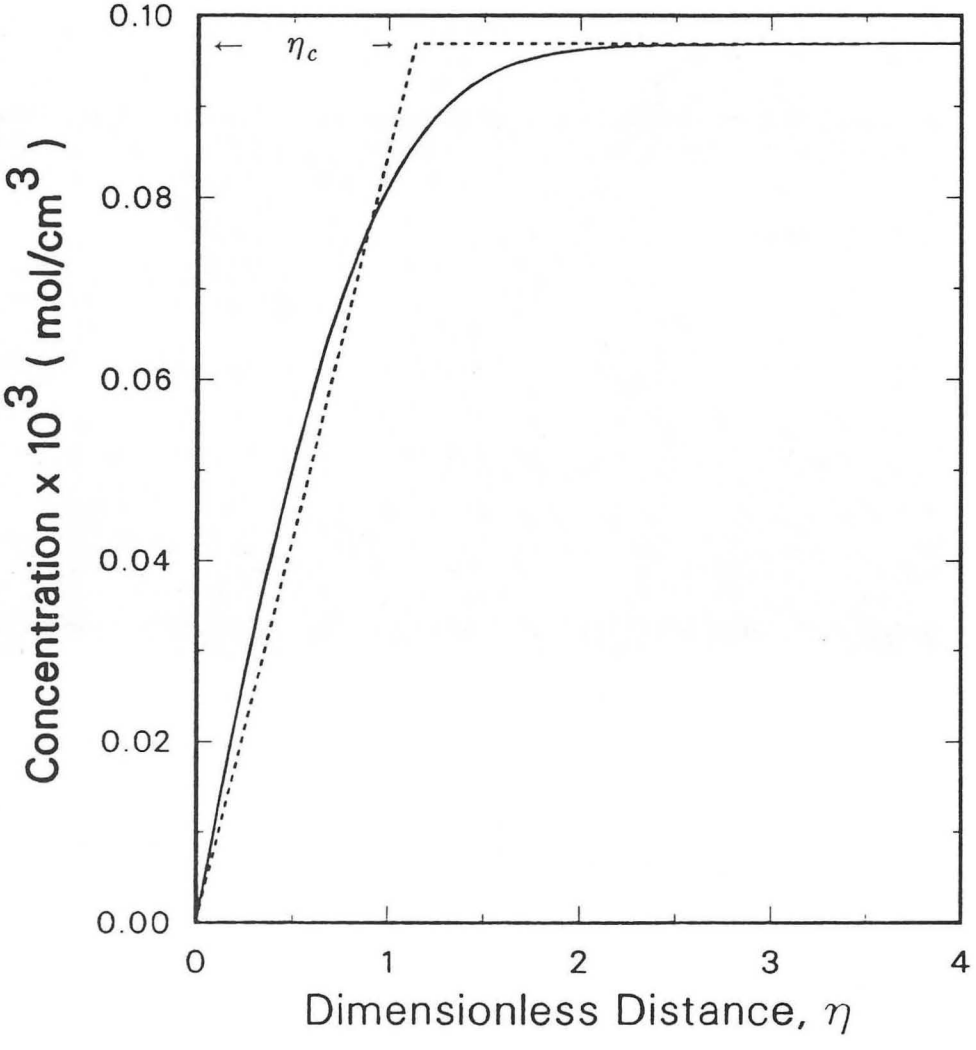

Figure 3. Calculated concentration profile of reactant Fe^{+3} following a potential step into limiting current. Dimensionless penetration length η_c is shown.

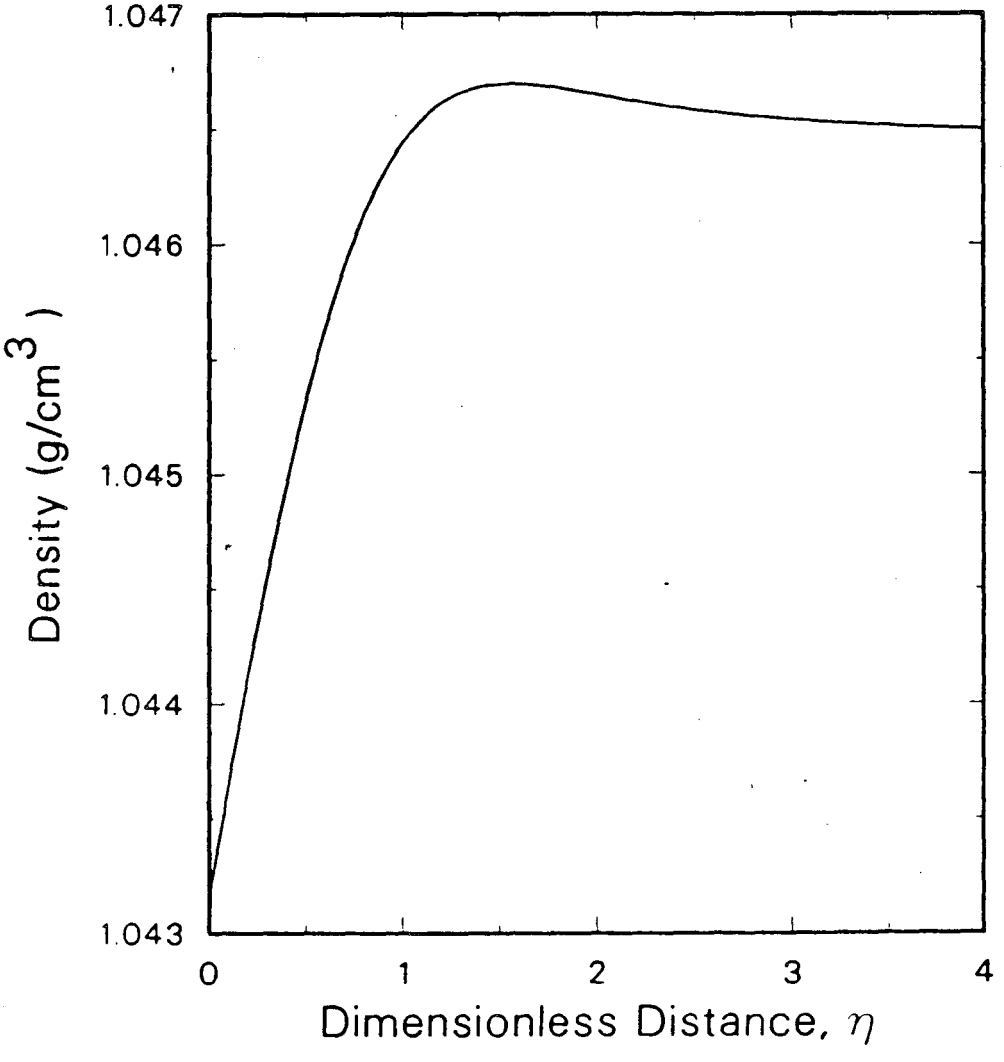

Figure 4. Calculated density profile following a potential step into limiting current.

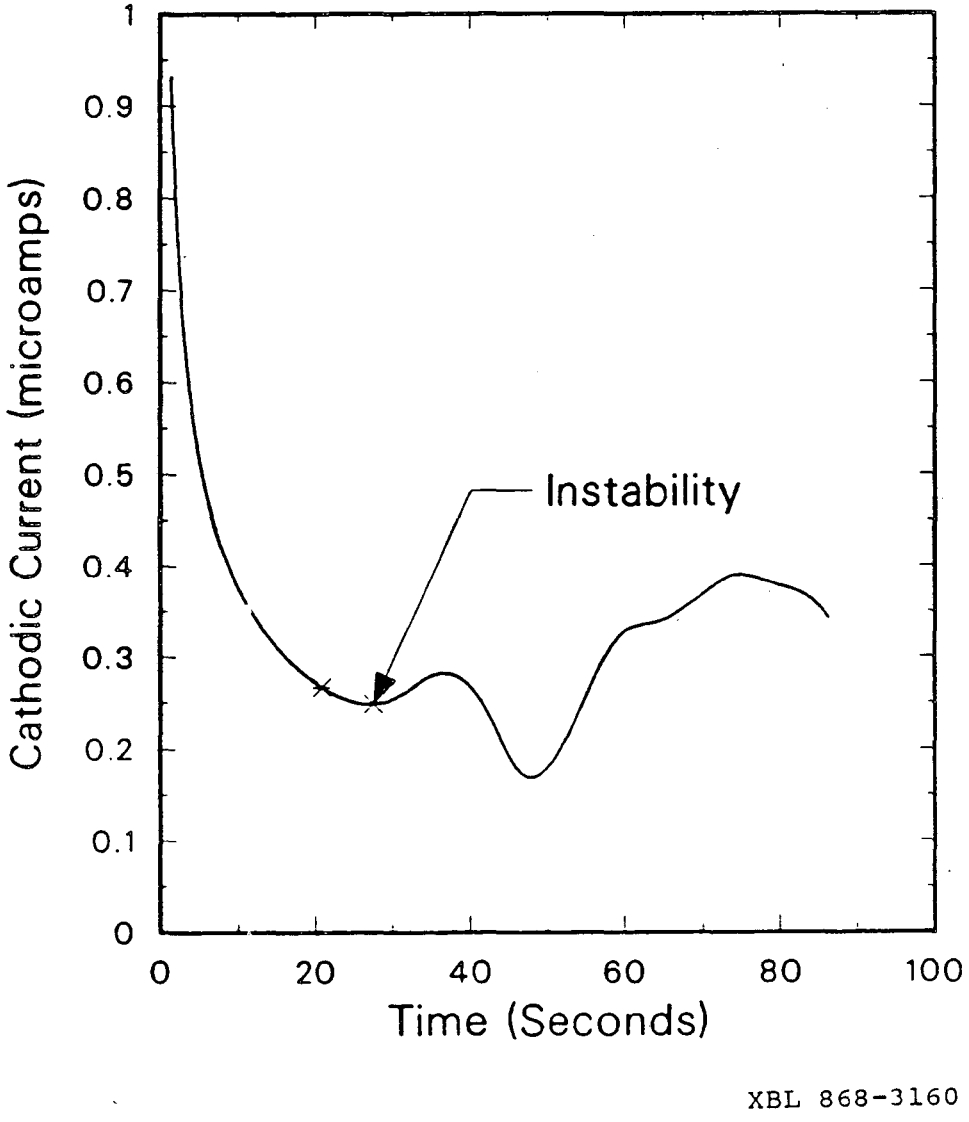

Figure 5. Current response of a single segment following a potential step into limiting current.

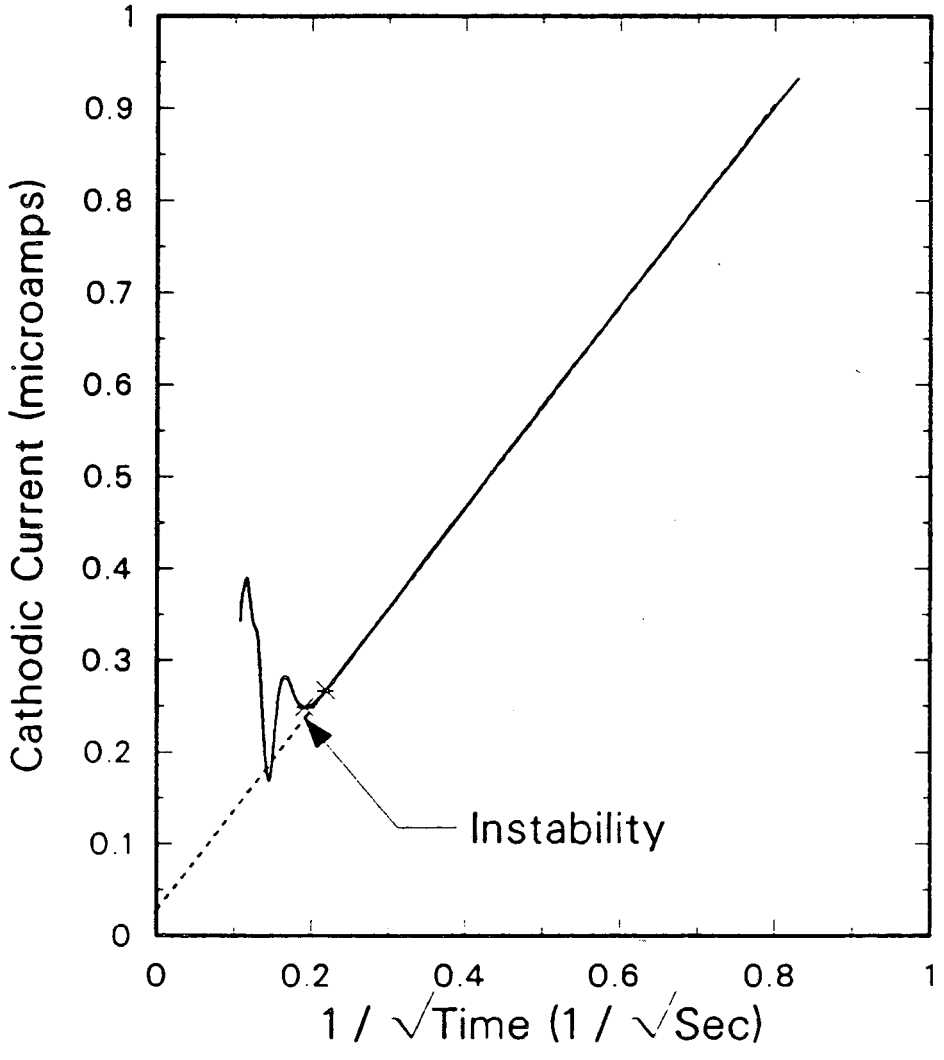

XBL 868-3161

Figure 6. Current response from Figure 5 plotted versus the inverse square root of time. The first (right) marker shows the last point used for calculating the diffusion coefficient. The second marker (left) shows the point of 5% deviation from linearity.

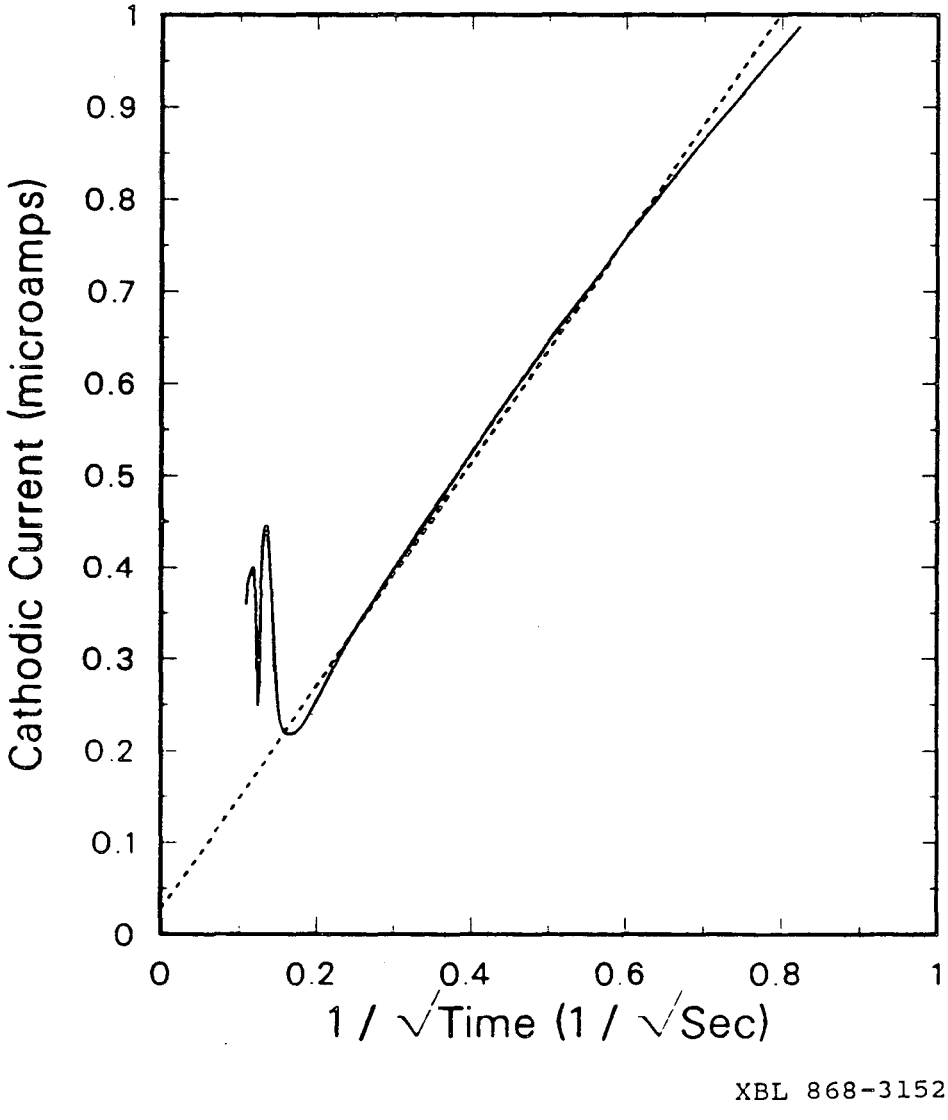

Figure 7. Current response of a single segment following a potential step into limiting current, showing curvature due to an adjacent non-working segment.

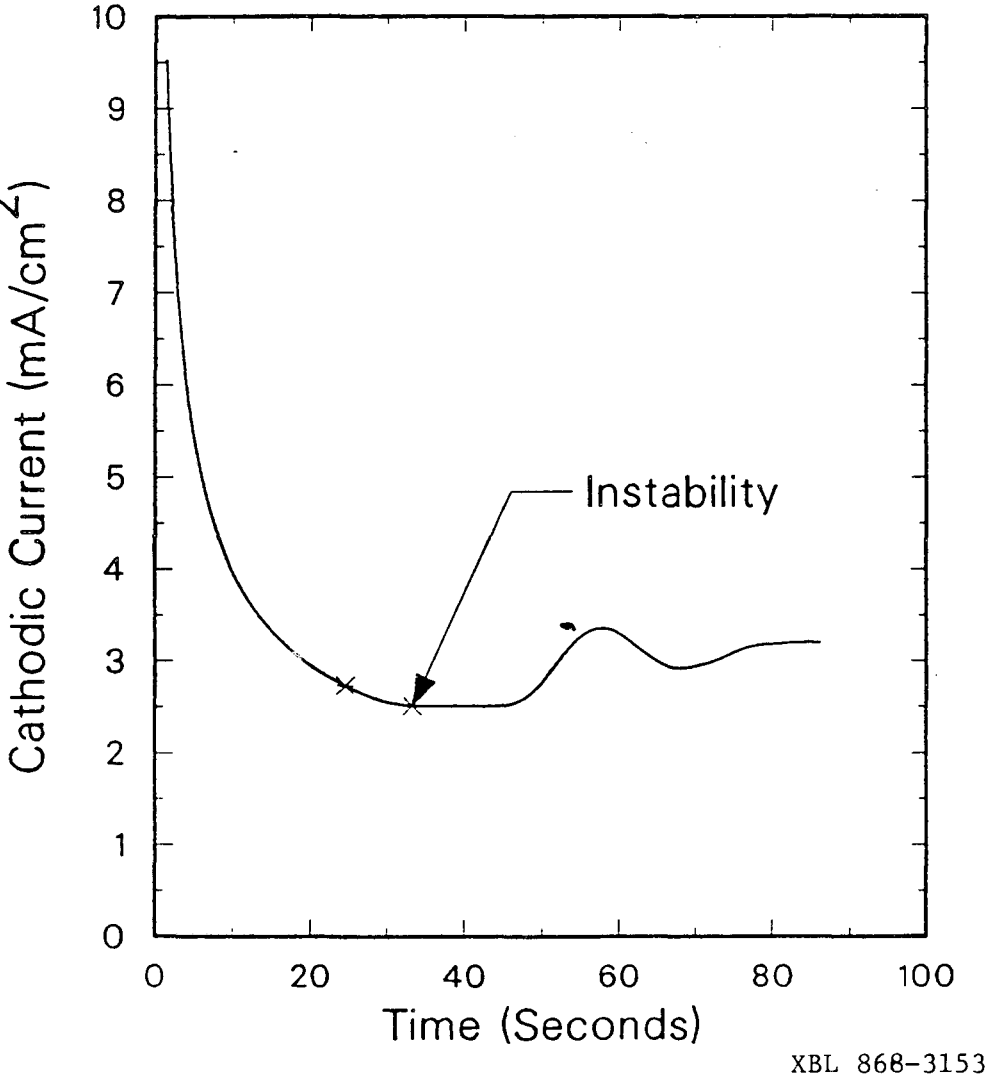

Figure 8. Total of the current responses obtained from all 55 segments following a potential step into limiting current.

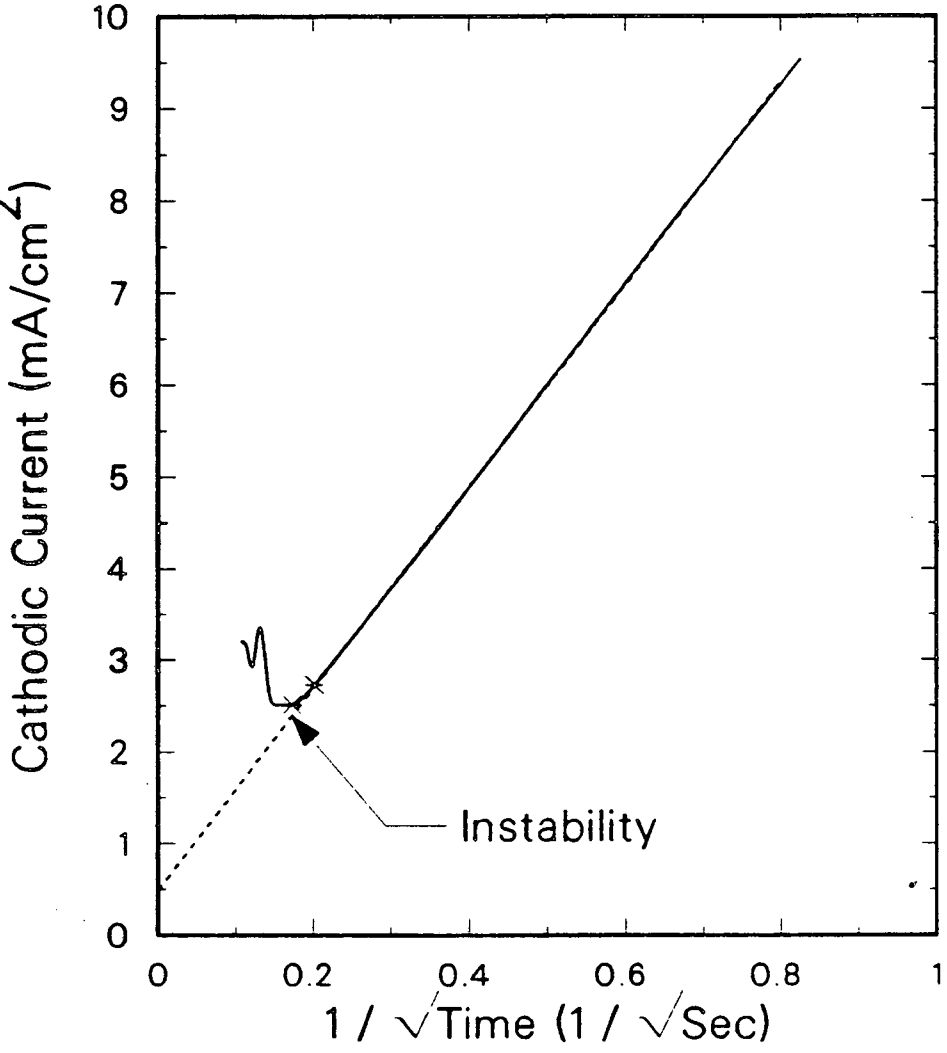

Figure 9. Inverse-square-root-of-time plot of the total current response obtained from all 55 segments following a potential step into limiting current.

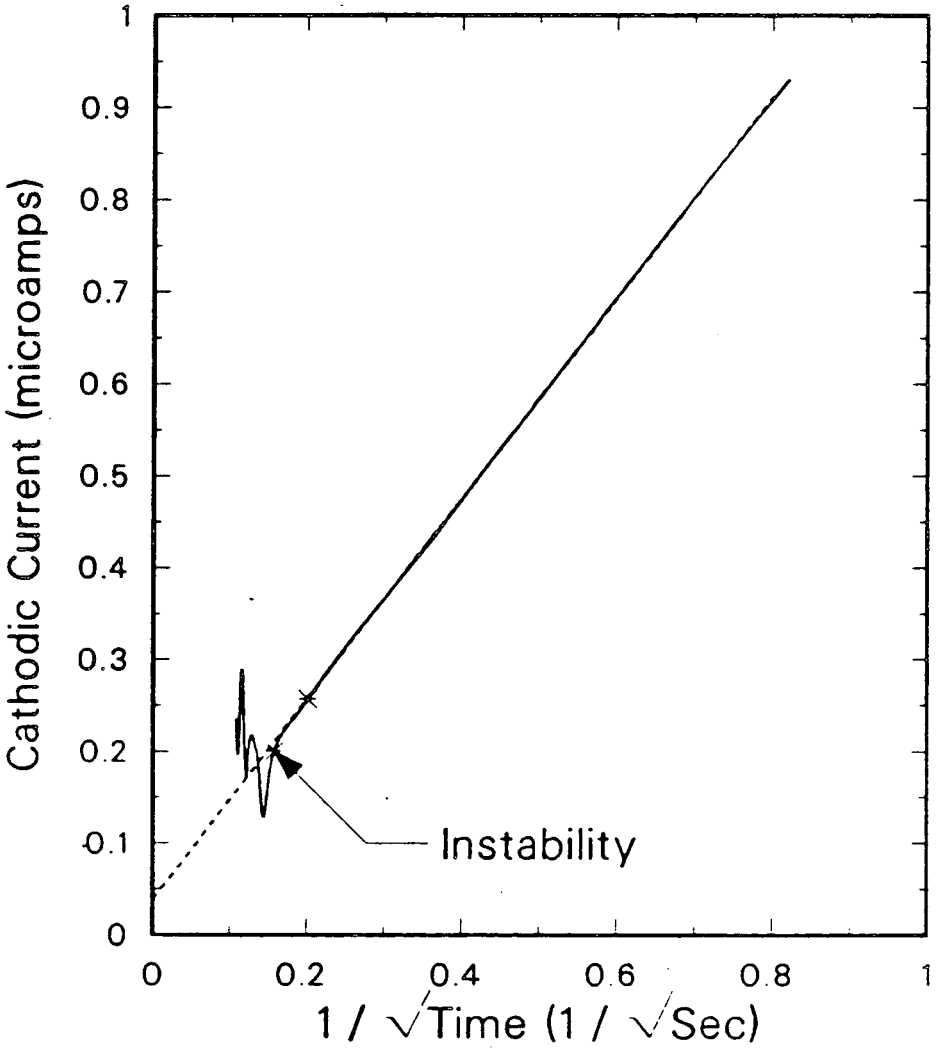

Figure 10. Current response of a single segment following a potential step into limiting current, showing a sharp decrease in Sh at the time of onset of convection.

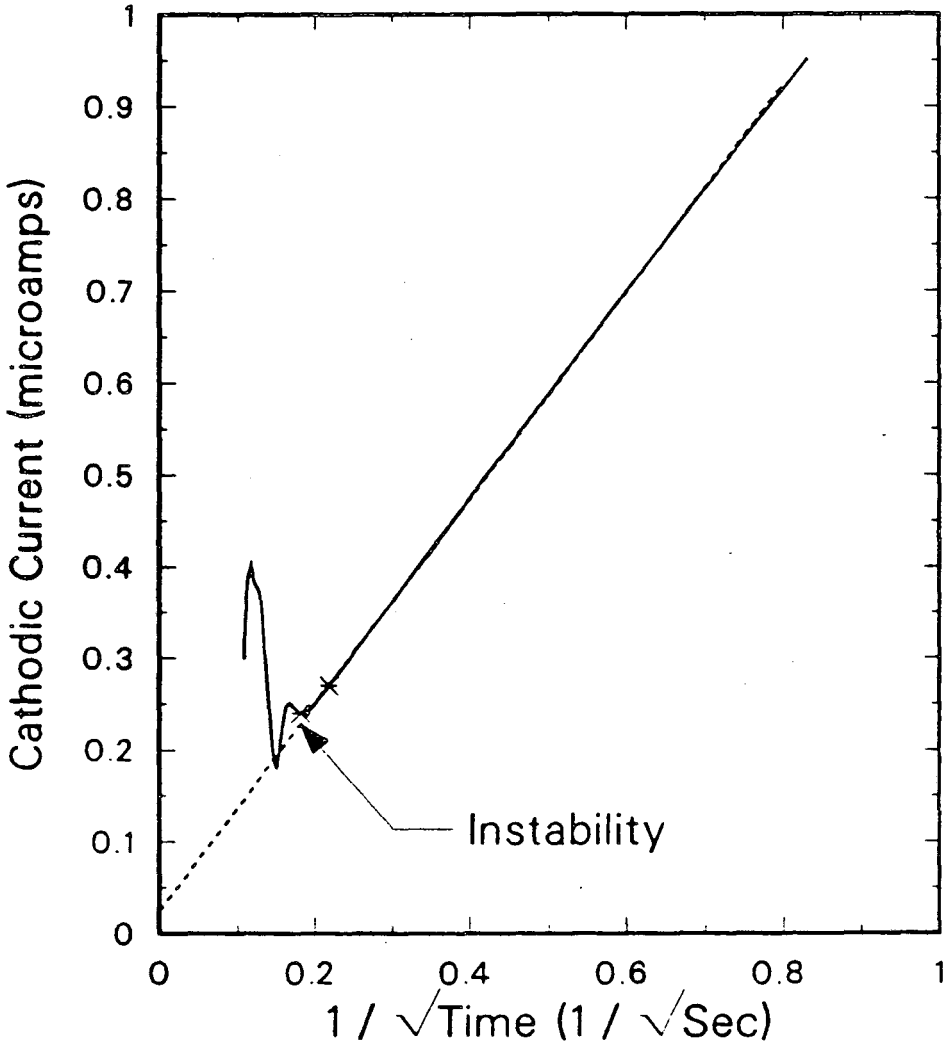

Figure 11. Current response of a segment following a potential step into limiting current, showing an *increase* in Sh at the time of onset of convection.

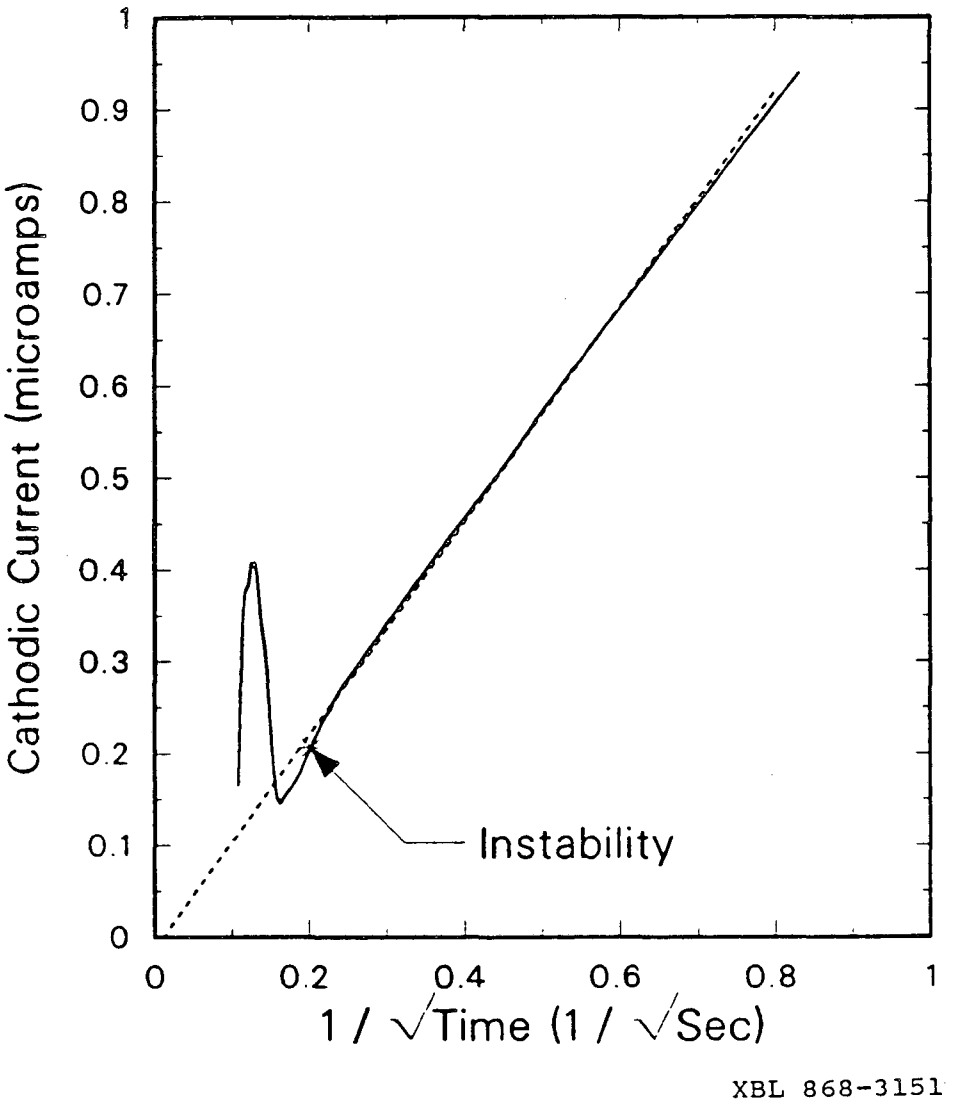

Figure 12. Current response of a segment which is 200 μm from that shown in Figure 11, exhibiting a *decrease* in Sh at the time of onset of convection.

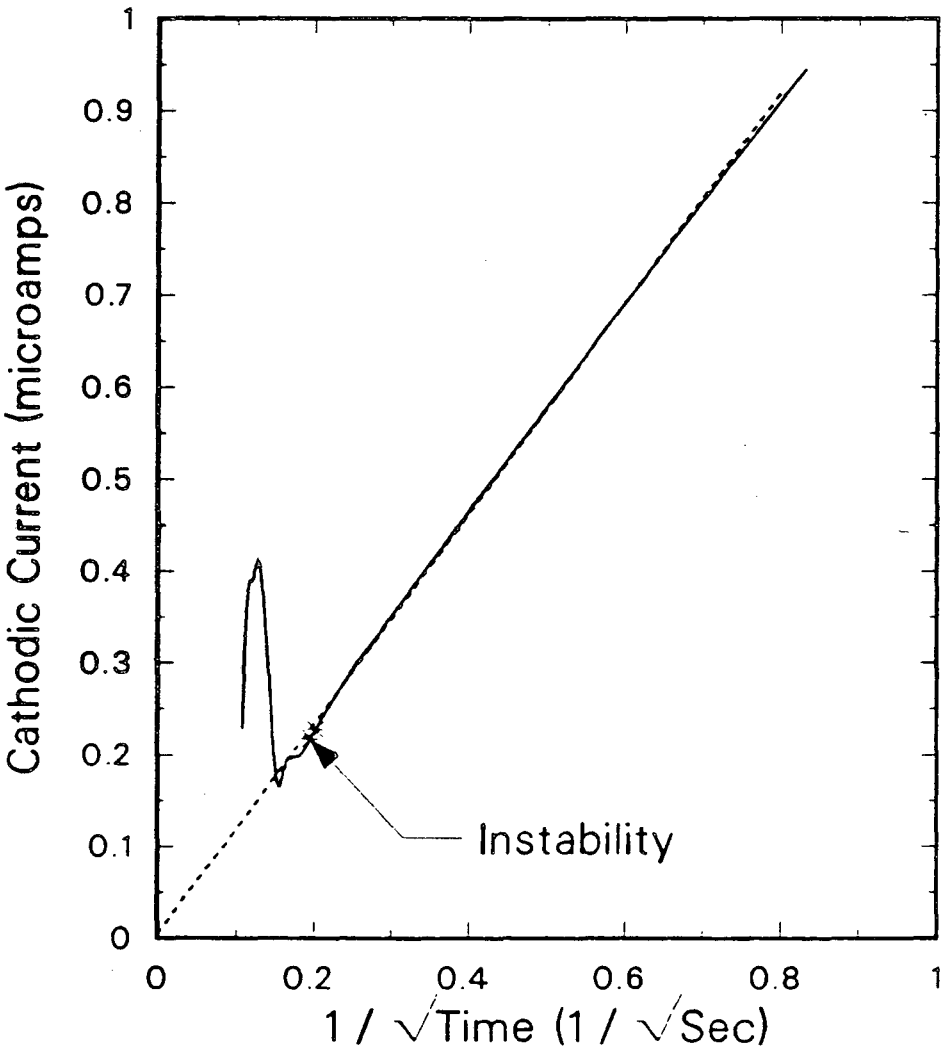

XBL 868-3157

Figure 13. Current response of the segment between the two shown in Figures 11 and 12, showing two slight decreases, followed by a large increase in Sh at the time of convection onset.

LAWRENCE BERKELEY LABORATORY
TECHNICAL INFORMATION DEPARTMENT
UNIVERSITY OF CALIFORNIA
BERKELEY, CALIFORNIA 94720